Contributions to Geophysics and Geodesy Vol. 42/1, 2012 (25–61)

Applying the regularized derivatives approach in Euler deconvolution and modeling geophysical data to estimate the deep active structures for the northern Red Sea Rift region, Egypt

Salah SALEH[1], Roman PAŠTEKA[2]

[1] National Research Institute of Astronomy and Geophysics
11421 Helwan, Cairo, Egypt; e-mail: salahsmm@yahoo.com

[2]Department of Applied and Environmental Geophysics, Faculty of Natural Sciences,
Comenius University, Mlynská dolina, 842 15 Bratislava, Slovak Republic
e-mail: pasteka@fns.uniba.sk

Abstract: The Red Sea is considered to be a typical example of a newly formed ocean. Moreover the northern Red Sea region and Gulf of Suez are generally important due to their hydrocarbon resources. Estimation of higher derivatives of potential fields represents a significant role in geophysical interpretation (qualitative and/or quantitative), as has been demonstrated in many approaches. One of the most popular methods, employing higher derivatives is the well known Euler deconvolution method. In this method it is very important to stabilize the derivatives evaluation, because they are very sensitive to noise and errors in the interpreted field. One way to stabilize higher derivative evaluation is the utilization of the Tikhonov regularization. We show the influence of regularized derivatives on the properties of the classical 3D Euler deconvolution algorithm and apply it to geophysical potential field data from the Red Sea Rift and its surroundings. The solution obtained with regularized derivatives gives better focused depth-estimates, which are closer to the real position of sources; the results presented here can be used to constrain depth to active crustal structures (boundaries and volcanisms) for northern Red Sea rift.

Estimated Euler solution map from Bouguer data utilizing the Tikhonov regularization reveals both the continental-oceanic crust boundary and several shallow listric normal faults spreading on the Red Sea margins having NW–SE direction, suggesting NE–SW extension in these regions. Also, generalized depth model for the structure of the Gulf of Aqaba (three pull-apart basins) was well recognized from this map. However, Euler solutions with band pass filter of magnetic data gives best depth-estimates connected with the volcanic intrusive bodies (intense magmatic activity) prevalent on and around the axial trough transform faults resulted from initiation of Red Sea Rift. This depth estimation was derived resulting different structural indexes (SI). The Majority of seismic epicenters along Red Sea rift is clustered on axial trough and on or near some active initiated transform faults of Red Sea basin which attributed to stresses from magmatic activity and rifting process.

doi: 10.2478/v10126-012-0003-x

Key words: regularized derivatives, Red Sea Rift, Bouguer anomaly map, aeromagnetic map

1. Introduction

The advancement in geophysical techniques leads to routine collection of magnetic and gravity datasets. The large data volume demands automatic techniques like Naudy *(Naudy, 1971)*, Euler *(Thompson, 1982)* and Werner deconvolution *(Werner, 1953)* for the interpretation of magnetic and gravity anomalies. Euler deconvolution has emerged as a powerful technique for estimating the depth and the geometry of the buried magnetic sources *(Thompson, 1982; Reid et al., 1990)*. This technique has become popular because it requires no a priori information about the source magnetization/density and it assumes no particular geological model. *Thompson (1982)* developed this technique for profile data while *Reid et al. (1990)* extended it for gridded data.

Semi-automated (classical Euler deconvolution) interpretation methods in applied magnetometry and gravimetry are based on estimation of source parameters directly from the measured (processed) and/or transformed potential fields. These methods are built on introduction of a priori information on the properties of the desired solution, mainly at the mathematical level. In the majority of cases, the a priori information is based on the recognition of a predefined source type response in the interpreted data. This approach does not fully solve the ambiguity of the inverse problem in potential field's interpretation. By means of this approach, we introduce into the solutions the so-called model error *(Dmitriev et al., 1990)* – this is connected with the problem of description of the complex real situations by simple models.

The problem of the instability of inverse problem solutions is manifested in these kinds of methods by a great sensitivity to the noise and errors in the interpreted fields. A large group of these interpretation methods use higher gradients of the interpreted field (e.g., Werner and Euler deconvolution, methods based on analytical signal evaluation, normalized derivative methods and many other approaches, e.g., *Nabighian (1972, 1974, 1984), Thompson (1982), Cooper and Cowan (2006), Nabighian and Hansen (2001), Salem and Ravat (2003), Hartman et al. (1971), Roest et*

al. (1992), Wijns et al. (2005), Reid et al. (1990), Mushayandebvu et al. (2001), Mushayandebvu et al. (2004), Salem et al. (2007) and many others.

The calculations of higher derivatives (gradients) of potential fields are unstable operations in the sense of mathematical physics definition and their incorrect evaluation can contribute to the enlargement of the instability of the whole method. The modulus of the complex spectral characteristics of the first horizontal (vertical) derivative in the Fourier domain is a linear function of the wave number – its application will amplify the spectral contents from higher wavenumbers (mainly the noise and errors in the original data). To obtain accurate values of numerically calculated derivatives, we need to damp this amplification of the high-frequency content in the processed signal.

In this paper, we attempt to map the subsurface structure and estimate the depth to deep structures in the northern Red Sea region using the existing geophysical data. This study is based on the application of gradient (Euler deconvolution and filtering) techniques. The advantage of these techniques is that they provide source location parameters using only a few assumptions. However, these methods evaluate different structural models such as contacts, sheets (dike and sills) and dipole, which may over-simplify the true situation.

2. Tectonics geological setting and seismicity

The Red Sea forms part of a rift system that includes the Gulf of Aden and East African Rift system in the south and the Gulf of Suez and Gulf of Aqaba in the north. The Red Sea and the Gulf of Aqaba were formed by upwarping of African-Arabian shield with its subsequent rifting, transform faulting and final break-apart, contrary to the Gulf of Suez, which was originated as a depositional realm that dates back to Early Paleozoic time *(Said, 1962)*.

At the north of the Red Sea the splits into the opening of the Gulf of Suez and the Gulf of Aqaba-Dead Sea rift system dominated by sinistral shear *(Ben-Menahem et al., 1976)*. Also, the Suez Rift is considered to be the plate boundary between the African and Sinai Subplate *(McKenzie et al., 1970; Francheteau and LePichon, 1972)*.

In general, it is accepted that the Gulf of Suez and Red Sea depressions were formed by the anti-clockwise rotation of Arabian Plate away from African Plate *(Cochran, 1983)*. Several geological and seismological investigations assert that the area surrounding the Gulf of Suez displayed, in the past, extensional tectonics with large deformation rate (e.g., *Ben-Menahem et al., 1976; Le Pichon and Gaulier, 1988; Steckler et al., 1988, 1998; Salamon et al., 1996; Piersanti et al., 2001*).

The tectonics of the Sinai Peninsula and the Gulf of Aqaba is strongly dominated by the active boundaries between the African and the Arabian plates that are separated from each other. According to the current literature, from Neogene to Late Miocene, this area was subjected to different phases of motion.

The oldest known formation in the study area is of Late Precambrian age, igneous and metamorphic rocks forming the northern edge of the African Shield (Fig. 1). The basement complex outcrops in southern Sinai and in the Eastern Desert (Red Sea mountain range). *Said (1962)* and *El-Gezeery and Marsouk (1974)* showed that the depth of the basement increases northwards towards the Mediterranean Sea. The Miocene was a period of great transformation, leading to the present Red Sea coast sediments and similar sedimentation in the north-western part of the Gulf of Suez. After the Oligocene uplift, an Early and Middle Miocene Tethys transgression began, only to be followed by late Miocene regression related to Alpine orogeny to the north. More extensive marine beds were formed in the Miocene, with a maximum extent in the Middle Miocene, when they reached to the Gulf of Suez and the Red Sea region beyond the Egyptian border. Pliocene sediments are widely distributed along the Red Sea. The Quaternary was characterized by regression with minor transgression. Uplift and tectonic disturbances mark the Pliocene-Quaternary boundary in the Red Sea region. Quaternary volcanism occurred in the Red Sea axial trough *(El-Gezeery and Marsouk, 1974)*.

High seismic activity along axial depression of Red Sea (mainly crustal source events) (Fig. 2) is mainly attributed to rifting process of the Red Sea. This seismic activity is due to rift extensional faults along axial depression accompanied with deep magmatic sources (volcanoes) especially those located on the oceanic-anomalous upper mantle contacts.

Korrat et al. (2006) studied the seismicity in the northernmost part of

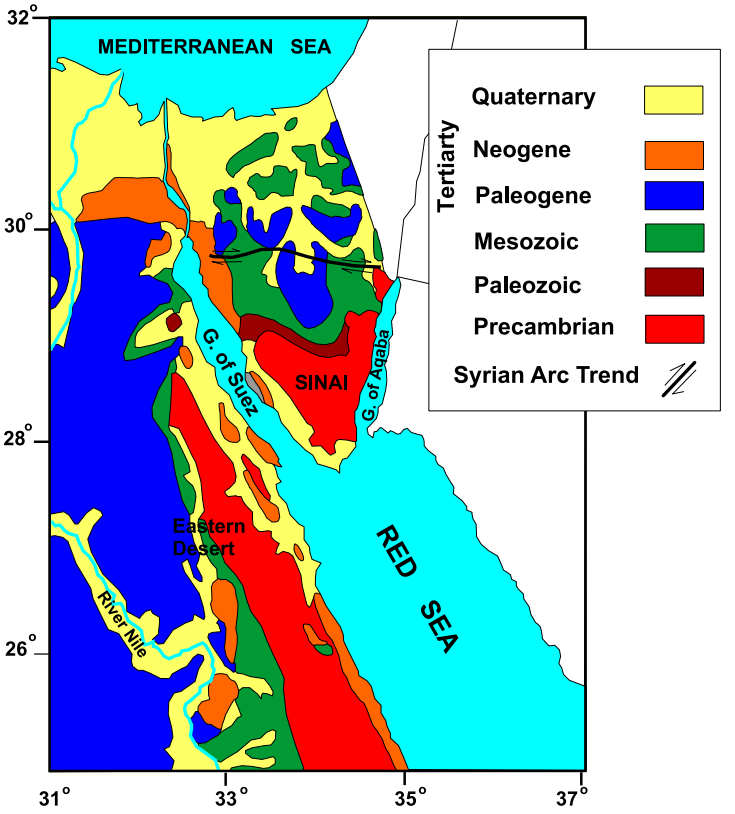

Fig. 1. Geological map for the region of study (from Egyptian Geological Survey, 1994).

the Red Sea using data from Hurghada Seismological Network and data from national centers in addition to readings from the existing neighboring networks to obtain a complete and true picture for the seismicity of the area. Their conclusions stated that, the spatial distribution of earthquakes defines three earthquake zones in the Gulf of Aqaba and three zones at the entrance of the Gulf of Suez and southern tip of Sinai Peninsula. The thermal activity and the triple junction nature control the activity in this area. The activity defines also an active trend extending from the southern tip of Sinai Peninsula to the median zone of the Red Sea. The seismicity of this trend is probably related to the active spreading zone associated with the opening of the Red Sea.

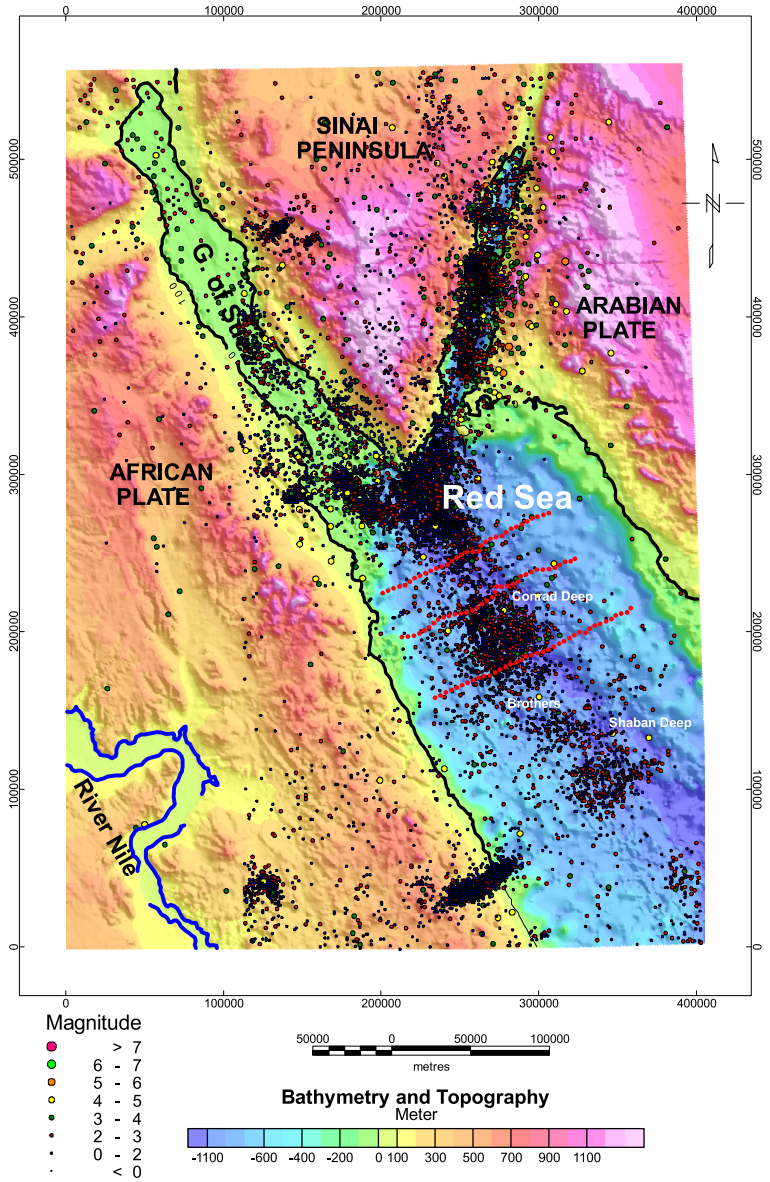

Fig. 2. Seismicity map of the studied region. It shows the earthquake activity in the northern Red Sea, (ISS files 1900-1963 and 1964-1998, NEIC files 1973-2010, and from Egyptian National Seismic Network (ENSN), 1998-2010). Location of heat flow profiles are shown in Fig. 3 is marked by aligned black dots.

Locating the earthquake activity (Fig. 2) shows high seismicity in the southern part of the Suez which is mainly attributed to the presence of Sinai triple junction *(Badawy et al., 2008)*. Also, rift extensional faults in the southern Gulf of Suez and juncture with the Gulf of Aqaba remained active in the Quaternary and to the present. This is evidenced by continued seismic activity *(Daggett et al., 1986; Jackson et al., 1988)*. Based on analysis of borehole breakout data from exploration wells and small-scale fault kinematics, the present-day orientation of the minimum horizontal stress is N15°E, approximately parallel to the Gulf of Aqaba–Levant transform boundary, and not perpendicular to the trend of the rift *(Bosworth and Taviani, 1996; Bosworth and Strecker, 1997)*.

3. Volcanism of northern Red Sea Rift

Almost no syn-rift volcanism has been reported from the exposed margins of the northern Red Sea rift. On the Sinai margin of the Gulf of Suez, the Abu Zenima formation (earliest syn-rift red beds) is capped by a basalt flow *(Plaziat et al., 1998; Bosworth and McClay, 2001)* that has been dated at 21 Ma. Other scattered dikes and flows in Sinai have been dated at 22–27 Ma *(Meneisy, 1990; Plaziat et al., 1998; Bosworth and McClay, 2001)* and a few basalt flows near Quseir (26°05″N) on the Egyptian Red Sea coast have been dated at 23–25 Ma *(Meneisy, 1990; Plaziat et al., 1998)*. After this early episode, rifting in the northern Red Sea appears to have been largely a magmatic. Diabase dikes and sills have been described from Zabargad (36°13′E and 23°33′N; e.g., *El Shazly et al., 1974; Bonatti et al., 1983; Nicolas et al., 1987; Bosworth et al., 1996*) and the Brothers Islands *(Shukri, 1944; Taviani et al., 1984)*. Both locations are uplifted slivers of crustal and mantle rocks, with prerift sedimentary rocks present on Zabargad (e.g., *Bonatti et al., 1983; Bosworth et al., 1996*).

Heat flow density in the Red Sea is generally high, reflecting the shallow depth to the asthenosphere and its recent age of intrusions. The early surveys, e.g. *Girdler (1970), Haenel (1972), Girdler and Evans (1977)*, reported high heat flow density values of approximately 600 mW/m^2 for the axial trough, whereas the flanks have values of twice the world mean (59 mW/m^2).

Martinez and Cochran (1988, 1989) presented three profiles of closely spaced heat flow measurements extending across the northern Red Sea (see location of heat flow profiles Fig. 2). In all three profiles, heat flow increases from about 125 mW/m^2 near the margins to 250–350 mW/m^2 in the axial depression (Fig. 3). The association of the maximum heat flow with the axial depression is particularly clear for the northern profile where the axial depression is offset towards the western portion of the Red Sea. *Buck et al. (1988)* and *Martinez and Cochran (1989)* modelled the heat flow resulting from different extension models including simple shear and a number of pure shear models in which the extending region either broadened with the rift or remained a constant width. They found that, to match the heat flow pattern, it is necessary that the zone of extension widen with the rift throughout most of the rifting history (for $\sim$ 20 myr), but narrows to a width comparable to the axial depression ($\sim$ 20 km) within the last 5 myr. These models also suggest that melt may have begun to be generated very recently under the axis *(Buck et al., 1988; Martinez and Cochran, 1989)*.

Cochran (2005) studied the magnetic anomalies of northern Red Sea. His results demonstrated small volcanoes which are normally magnetized and thus presumably have been erupted since 780 ka. These volcanoes are systematically located relative to the rift structure. They occur at the top of scarps or slopes marking the edge of terraces and appear to have ascended through the crust along faults.

4. Geophysical data

4.1. Gravity data

A considerable amount of gravity data base is now available to unravel the subsurface structure of the Red Sea region. In order to investigate the structure of the northern Red Sea rift and Gulf of Suez, modified Bouguer gravity anomaly map has been prepared. It utilizes all available gravity data: Bouguer gravity data of the Egyptian General Petroleum Company published as a set of Bouguer maps of Egypt at 1:500 000 scale in 1980; gravity surveys of the Gulf of Suez, Sinai and the Eastern Desert conducted by the Sahara Petroleum Company (SAPETCO) and PHILIPS Company

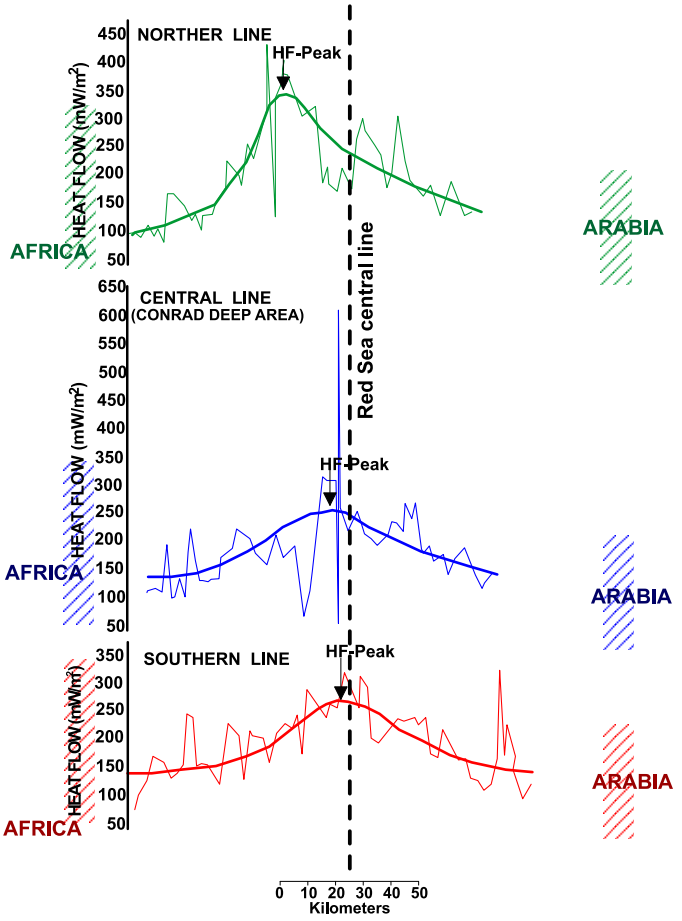

Fig. 3. Heat flow profiles across the northern Red Sea. Location of the measurements is shown in Fig. 2. Bathymetry and heat flow data are projected along an azimuth of N60°E modified from Martinez and Cochran (1989).

between 1954 and 1958; marine gravity data in the northern Red Sea measured by the research vessel "Robert D. Conrad" to the north of 26°N in 1984. All the data of these surveys were compiled, classified and ranked according to instrument sensitivity and measurement density. More details on how the Bouguer map was compiled can be found in *Saleh et al. (2006)*. The resulting Bouguer map is shown in Fig. 4. The calculated

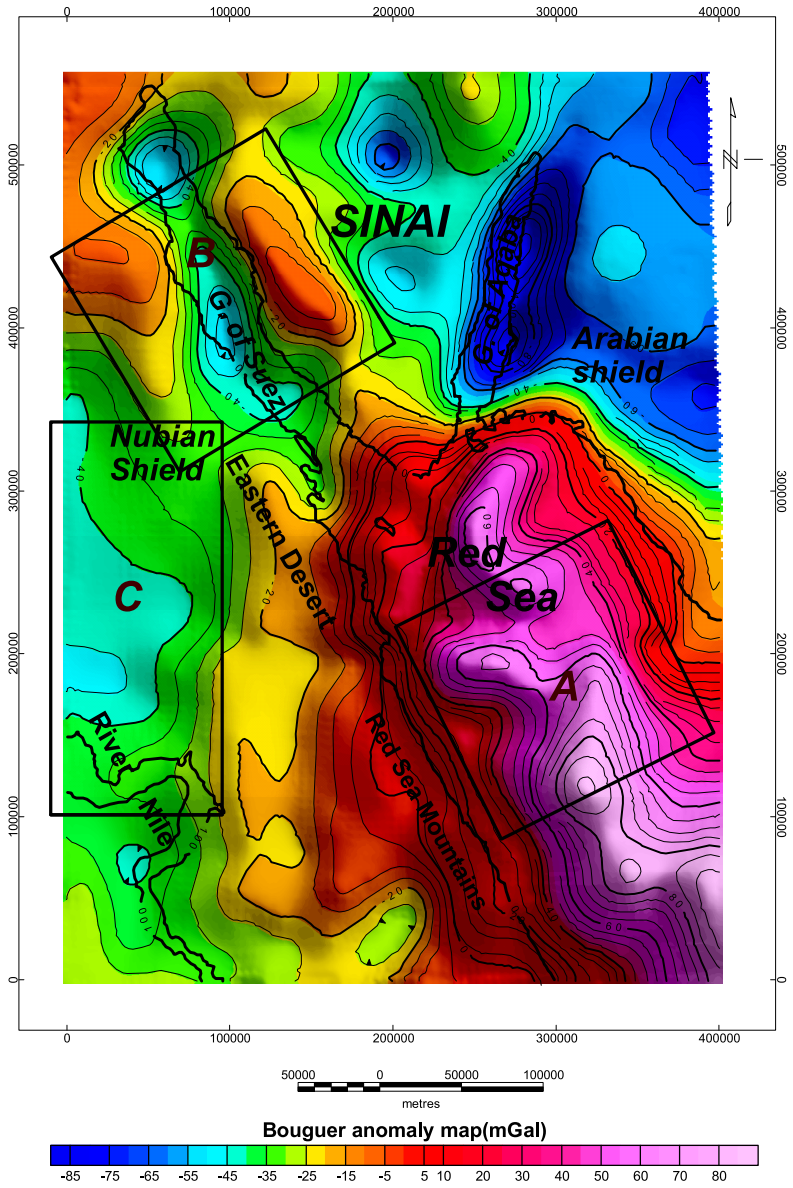

Fig. 4. Measured Bouguer anomaly map of the Red Sea and surrounding region. Contour interval is 5 mGal. Density of reduction is 2.67 g/cm^3 and the international gravity formula of 1967 has been used. The topographic corrections have been applied. (Modified after the GPC, Cairo, 1980).

Bouguer gravity anomaly is corrected for mass effects of topography with the standard density of reduction 2670 kg/m^3. The general trend of the Bouguer gravity anomalies is northwest–southeast. The anomaly increases in magnitude with a decrease in the relief of the topography and attains its maximum of +95 mGal along the axis of the Red Sea rift floor. A systematic slight decrease of the amplitude occures to the north; where the maximum amplitude is of the order 80 mGal south the interance of Gulf of Aqaba. The highest mountains in the Red Sea Ranges for example have values of over 1000 m, and their negative Bouguer anomalies are only about −10 to −30 mGal, aligned parallel to the Red Sea along a NNW trend.

Alternative negative and positive anomalies along the Gulf of Suez (region B) may be due to the faulted blocks or presence of different basins with different thickness of sedimentary sequence in the area. This leads to the conclusion that the shallow parts are extending along the two Gulfs and southern part of Sinai where the basement rocks are outcropping (Fig. 4).

It was observed an elongated anomaly with gravity value between −35 and −50 mGals extended from 26 to 28.5 N and 31.5 to 33 E (region C). The elevation of this area is fairly smooth and only 200 to 400 m above sea level.

The Red Sea Mountains with altitudes over 800 m show Bouguer anomalies between −10 mGals and −35 mGals, the values increasing to zero gravity level at the Red Sea coast. These anomalies suggest that the crust attains its maximum thickness below the Red Sea Mountains and thins considerably towards the Red Sea Rift. In the Red Sea, the anomalies are positive; the anomaly increases in magnitude with a decrease in the relief of the topography and attains its maximum of +80 mGal along the axis of the Red Sea Rift floor. In eastern Egypt and the Gulf of Suez, the anomalies have a NNW-SSE trend which is associated with the Miocene and Post Miocene opening of the Red Sea and Gulf of Suez.

4.2. Magnetic data

The marine aeromagnetic map was compiled for both the Gulf of Suez and the northern Red Sea based on *Cochran et al. (1986)* and *Meshref (1990)*. The total magnetic intensity data resulting from different aeromagnetic surveys was compiled and reduced to one set of data. The field has

been reduced to the pole *(Baranov, 1957)*, a regional magnetic effect has been subtracted (see *Saleh et al., 2006*). Magnetic data is available for a smaller area, than in the gravitational case. The resulting total magnetic intensity map is shown in Fig. 5. Both Bouguer and total intensity aeromagnetic anomaly maps (Figs. 4 and 5) indicate that most anomalies are aligned to NW, NE, and EW directions.

The total intensity magnetic anomaly map (Fig. 5) shows a pattern of magnetic anomalies within the marine portion of the northern Red Sea which exhibits a relatively flat magnetic field on which a number of large-amplitude dipolar anomalies are superimposed. Magnetic anomalies in the northern Red Sea are all dipolar anomalies (Fig. 5) implying a compact localized source.

These anomalies have been interpreted as arising from discrete localized volcanoes *(Cochran et al., 1986; Martinez and Cochran, 1988; Guennoc et al., 1988)*. The dipole type magmatic anomalies are concentrated to the axial depression (Fig. 5). Their magnetic field is orientated normal to the recent global magnetic field. This indicates that the corresponding magmatic intrusions are not older than 0.7 Ma *(Guennoc et al., 1988)* and could be as young as 40 ka *(Cochran et al., 1986)*.

5. Geophysical data analysis

Our data interpretation methods generally focus on the application of numerically evaluated gradients (Euler deconvolution and bandpass filter) techniques. In this paper, we propose to estimate both the source location and its depth which reveals the subsurface structures of studied region.

There are many classical procedures for the smoothing of evaluated gradients in the space domain (e.g., the Hamming window) or low-pass filtering in the Fourier domain (e.g., the Butterworth filter) but a simple "uncontrolled" smoothing of the derivatives seems to be insufficient – for a correct calculation of depth-estimates we need accurate values of the adopted derivatives. More sophisticated methods utilize the Wiener optimum filtering approach (e.g., *Pawlowski and Hansen, 1990*) or enhanced derivatives *(Fedi and Florio, 2001)*. There also exists a very elegant and straightforward method to solve this problem – the Tikhonov regularization *(Tikhonov and Arsenin,*

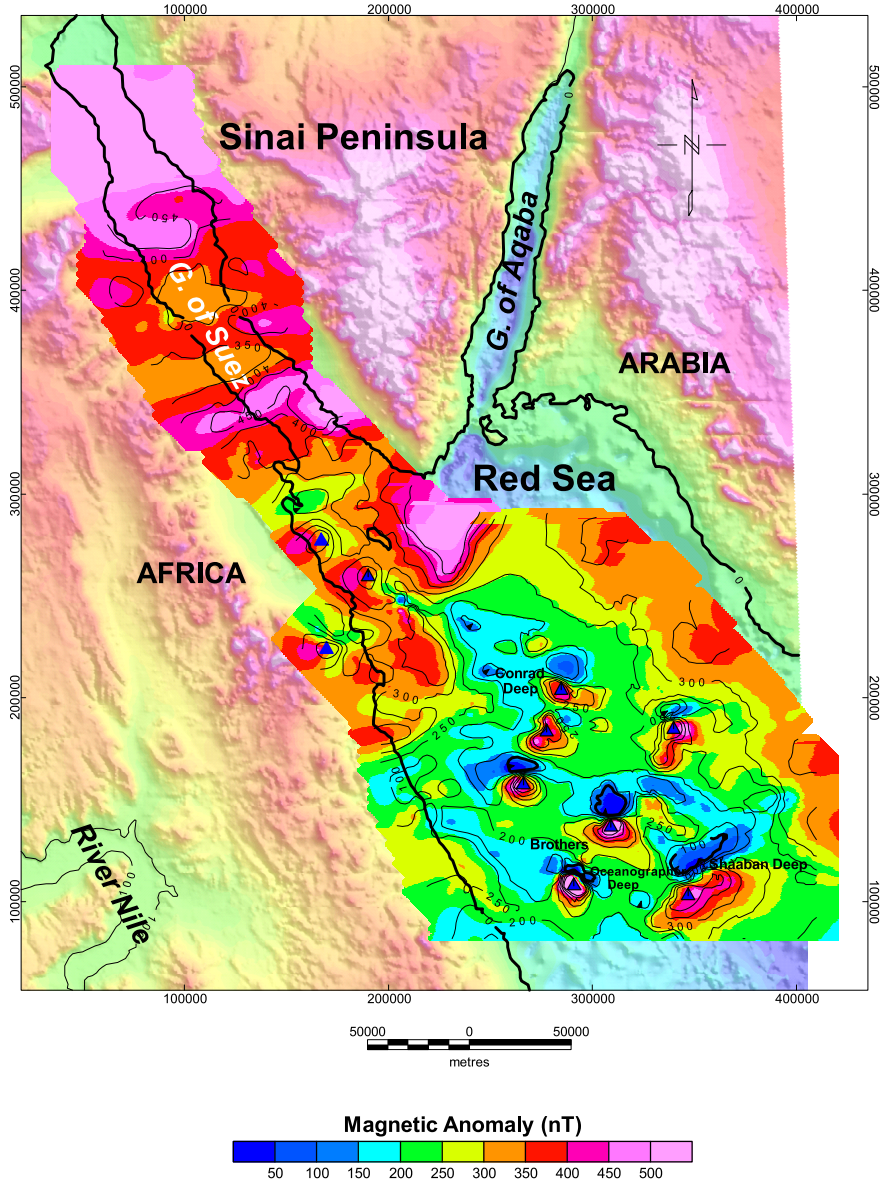

Fig. 5. Total intensity magnetic anomaly map of the northern Red Sea contoured at 50 nT intervals. Blue triangles mark location of volcanoes identified from magnetic anomalies.

1977).

This approach contributes to the solution of the discussed topic in two important ways: a) direct derivation of a low-pass filter in the Fourier domain for this type of problems and b) giving a method for the selection of an optimum filter parameter (in this case the so-called regularization parameter), which adapts the low-pass filter individually to each processed data set *(Pašteka et al., 2009).*

Here, the selection of the optimum regularization parameter plays a crucial role. In the application section we try to demonstrate the improvement of the properties of classical Euler deconvolution with regularized derivations, applied to high-definition potential field data of northern Red Sea rift.

The geophysical data is also filtered as a qualitative aspect of interpretation using bandpass filter. Both 3D Euler deconvolution and bandpass filter was successfully used beside. The objective of Euler deconvolution and filtering is to condition a data set and to render the resulting presentation in such a way as to make it easier for interpreting the significance of anomalies in terms of their geologic cause and setting. This operation can be performed several ways through manual/or automatic techniques. The most effective way to filter is with an understanding of the geologic control and an idea of the desired filtered results. In general, filtering data is powerful tool and often leads to important conclusions, but its use should be related to the nature of the geologic problem to be solved. 3D Euler deconvolution with the filtered bandpass maps, were used to trace easily the faults and/or any volcanic source bodies with estimation their depths investigations that characterized the study rift region. The results were compared with the available information, such as seismicity, geothermal geology, drilling holes, 3D gravity modeling map, which were available in the study area.

5.1. Euler deconvolution

5.1.1. Methodology

This semi-automated interpretation method is based on the utilization of the Euler's homogeneous functions theorem *(Thompson, 1982; Reid et al., 1990)* and belongs to the most popular and wide-spread depth-estimation

approaches. Euler deconvolution method (ED) is exploiting calculated higher derivatives of the interpreted field and a special source parameter – so-called structural index (SI), which is connected with the homogeneity degree of the source describing potential field function. For the total field magnetometry following values for different recognized structures are valid: 3 – dipole (sphere); 2 – cylinder (vertical or horizontal); 1 – sheet (sill or dike) and 0 – contact (large step). In the classical version of the SI method value was predefined by the interpreter and source-depth estimations (x_0, y_0, z_0) are obtained by means of the solution of the Euler equation (in a selected window):

$$(x - x_0)\frac{\partial \Delta T}{\partial x} + (y - y_0)\frac{\partial \Delta T}{\partial y} + (z - z_0)\frac{\partial \Delta T}{\partial z} = -SI\,(\Delta T - B)\,, \qquad (1)$$

where $\Delta T(x, y, z)$ is the interpreted anomalous magnetic field; x_0, y_0, z_0 are the coordinates of the searched source, B is a constant background field introduced by *Thompson (1982)* and SI is the mentioned structural index value (predefined by the interpreter).

In some newer modifications (e.g., *Mushayandebvu et al., 2001; Nabighian and Hansen, 2001; Hsu, 2002; Fedi and Florio, 2002; FitzGerald et al., 2004*) structural index value is obtained parallel with the determination of source positions, which represent an important development in the Euler methodology. In this paper, we have applied the so-called Derivative Euler Deconvolution (DED) *(Hsu, 2002; Fedi and Florio, 2002)*, which is based on the idea of employment the vertical derivative $\Delta T_z (= \partial \Delta T/\partial z)$ instead of the original ΔT field itself. The main reason is based on a need of canceling the "troublesome" non-linear combination of two unknowns SI·B in Eq. 1. Now we get a modified interpretation equation (where the constant background term B was canceled by means of the derivative evaluation):

$$(x - x_0)\frac{\partial \Delta T_z}{\partial x} + (y - y_0)\frac{\partial \Delta T_z}{\partial y} + (z - z_0)\frac{\partial \Delta T_z}{\partial z} = -SI_z \Delta T_z, \qquad (2)$$

where SI_z is the modified structural index, valid for vertical derivatives: SI_z = SI + 1 (showed systematically by *Stavrev, 1997* and *Stavrev and Reid, 2007*). This equation is defined for several points in a selected profile/grid window and solved in a linear system in the same way, like it was in the case of Eq. 1); in our case by means of the singular value decomposition

method. Obtained structural index values are increased by 1, because for final interpretation reasons it is better to use the standard SI values, used in magnetometry. Utilization of higher derivatives (in DED algorithm even more – by the evaluation of the initial vertical derivative ΔT_z) can lead to instability problems in the Euler deconvolution methodology – the method core is very sensitive to errors and noise in original interpreted data, which are amplified by derivatives evaluation. Because of this reason, we have used the stable derivatives evaluation by means of the Tikhonov regularization approach *(Pašteka et al., 2009)* – during the initial vertical derivative evaluation and also for the consecutive higher orthogonal derivatives calculation.

5.1.2. Magnetic source structures

5.1.2.1. Interpretation of 3D Euler deconvolution with regularized derivative

We have applied the proposed algorithm to the total magnetic field and Bouguer anomaly data from the northern Red Sea (Figs. 4 and 5). The magnetic field anomaly is predominantly due to Precambrian basement faults and magmatic intrusions. The magnetic data was collected along several profiles oriented in NNE-SSW direction. The Structural Index (SI) is assumed to vary between -0.5 to and 3.5 encompassing all plausible geological bodies. The estimates of source location, depth, SI and the statistical parameters are obtained by minimizing the error function using DED modification *(Hsu, 2002; Fedi and Florio, 2002)*.

The structural index η depends on the nature of the source. The 3D of Euler results are divided into several files, based on the estimated value of structural index (SI). For example, $\eta = 0$ (from -0.5 to 0.5) for a simple contact, $\eta = 1$ (from 0.5 to 1.5) for the top of a vertical dike or the edge of a sill, $\eta = 2$ (from 1.5 to 2.5) for the center of a horizontal or vertical cylinder, and $\eta = 3$ (from 2.5 to 3.5) for the center of a magnetic sphere or a dipole *(Thompson, 1982; Reid et al., 1990)*.

In this study, the Euler method has been applied assuming three models (contact, dike and dipole) with a moving window of 10×10 data points to locate the possible subsurface structures from the observed aeromagnetic data. Figures 6, 7 and 8 show the Euler solutions for each case (contact, dike, and dipole respectively). Most of the contact and dike solutions are

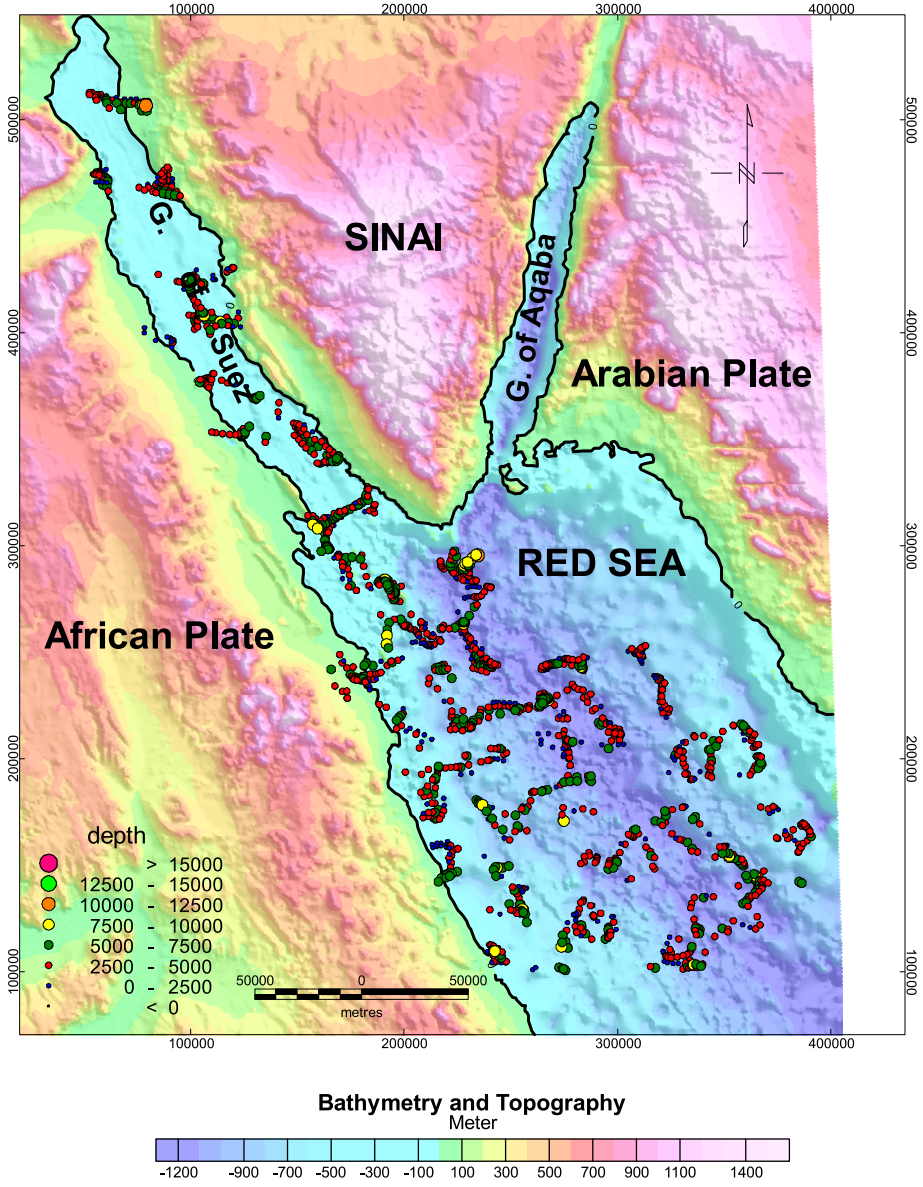

Fig. 6. Solutions of the 3D Euler method from the DED modification (Derivative Euler Deconvolution) for magnetic data resulting structural index of contact model.

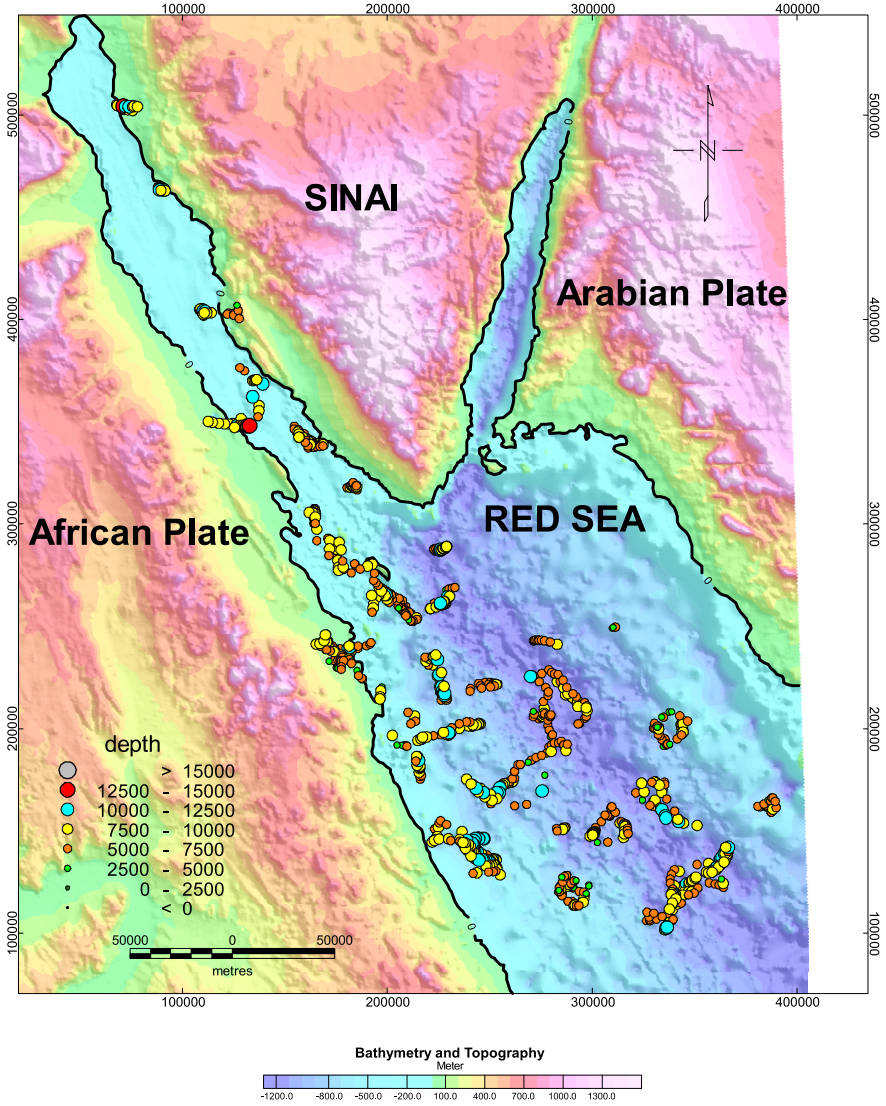

DED_3DEuler solutions_magnetic_sheets_Red Sea

Fig. 7. Solutions of the 3D Euler method from the DED modification (Derivative Euler Deconvolution) for magnetic data resulting structural index of sheet (dike and sills) model.

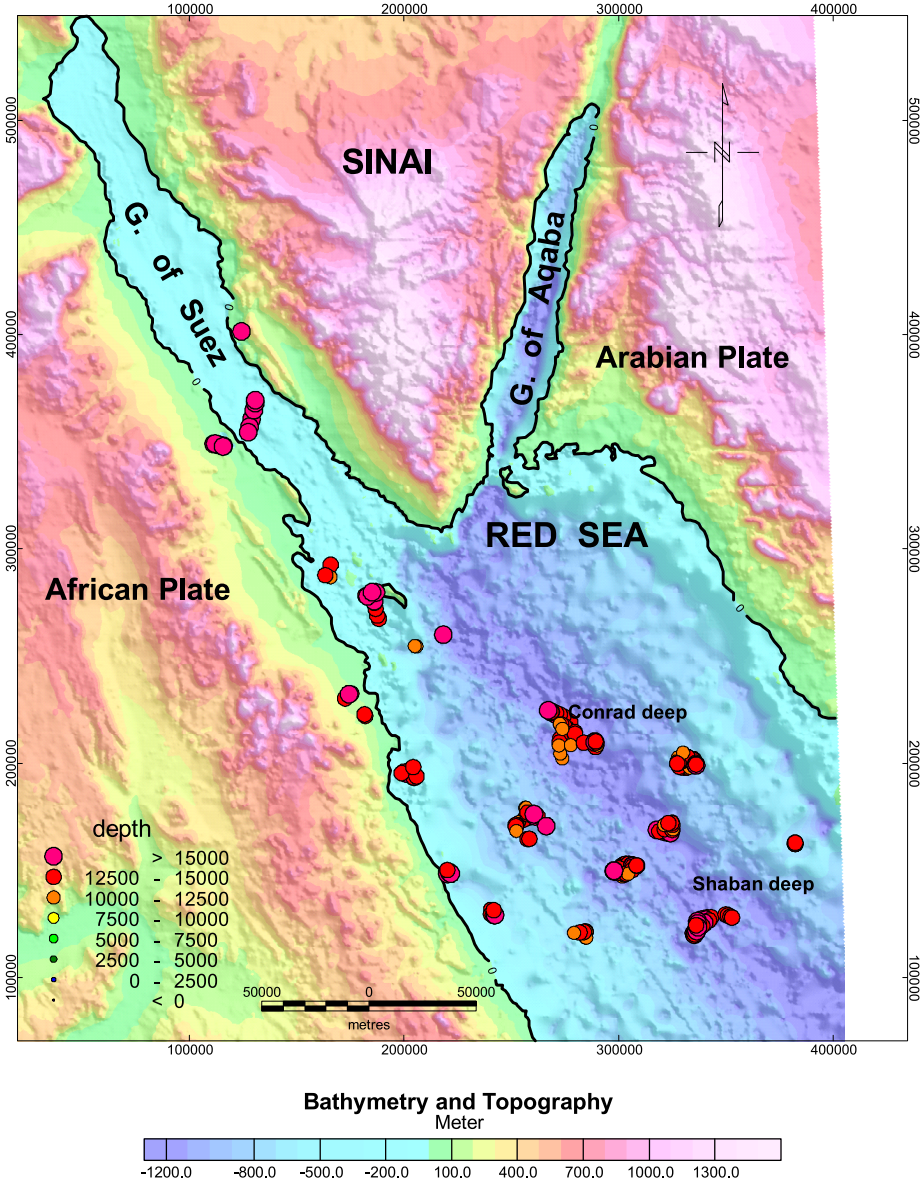

Fig. 8. Solutions of the 3D Euler method from the DED modification (Derivative Euler Deconvolution) for magnetic data resulting structural index of dipole model.

trending in the NNW and NW directions, associated approximately with the main trend of the Red Sea. In many locations with the dike and dipole models (Figs. 7 and 8), solutions are found to be trending in the NE–SW direction. This trend is related to the transformed faults, which is associated with the Red Sea rifting *(Said, 1962)*.

Generally, the magnetic field over the northern Red Sea takes the form of low amplitude, long wavelength variations on which a number of high amplitude, short wavelength anomalies caused by recent intrusion are superimposed *(Cochran and Martinez, 1988)*. The strong amplitude of these anomalies suggests that the causatives sources are diabasic dikes and probably have a genetic relation to the thermal system of the Red Sea. This expectation was reinforced by the field observations, which indicated that the basement rocks on the onshore part of the study are intensively intruded by diabasic dikes trending in the NNW and NW directions *(Abuzeid, 1988)*. Moreover, the mean investigated depth values of volcanic intrusive bodies (dipole model) were well defined and estimated using Euler deconvolution (utilization of the Tikhonov regularization of derivatives evaluation). These values are ranging from 10 to more than 18 km (Fig. 8), indicating that their source is the heated anomalous upper mantle *(Saleh et al., 2006)*, which consequently confirms the idea that the asthenospheric upwelling might be responsible for the subsequent rifting of the Red Sea.

5.1.2.2. BandPass magnetic map

The enhancement of magnetic anomalies associated with faults and other structural discontinuities was achieved by the application of bandpass filter of the TMI data. Bandpass filter parameters have been selected (1–7 km) after extensive testing of several bandpass ranges using Geosoft software (Oasis montaj version 6.3) to find one which provides the best continuity and resolution. Figure 9 show the bandpass filtered map, of TMI magnetic map overlain with interpreted faults and intrusions.

5.1.2.3. Transform faults

Both Euler deconvolution and Bandpass maps (Figs. 6, 7, 8 and 9) show several discontinuities separating the linear magnetic anomalies. These zones may represent fracture zones; transform faults, or regions in which the for-

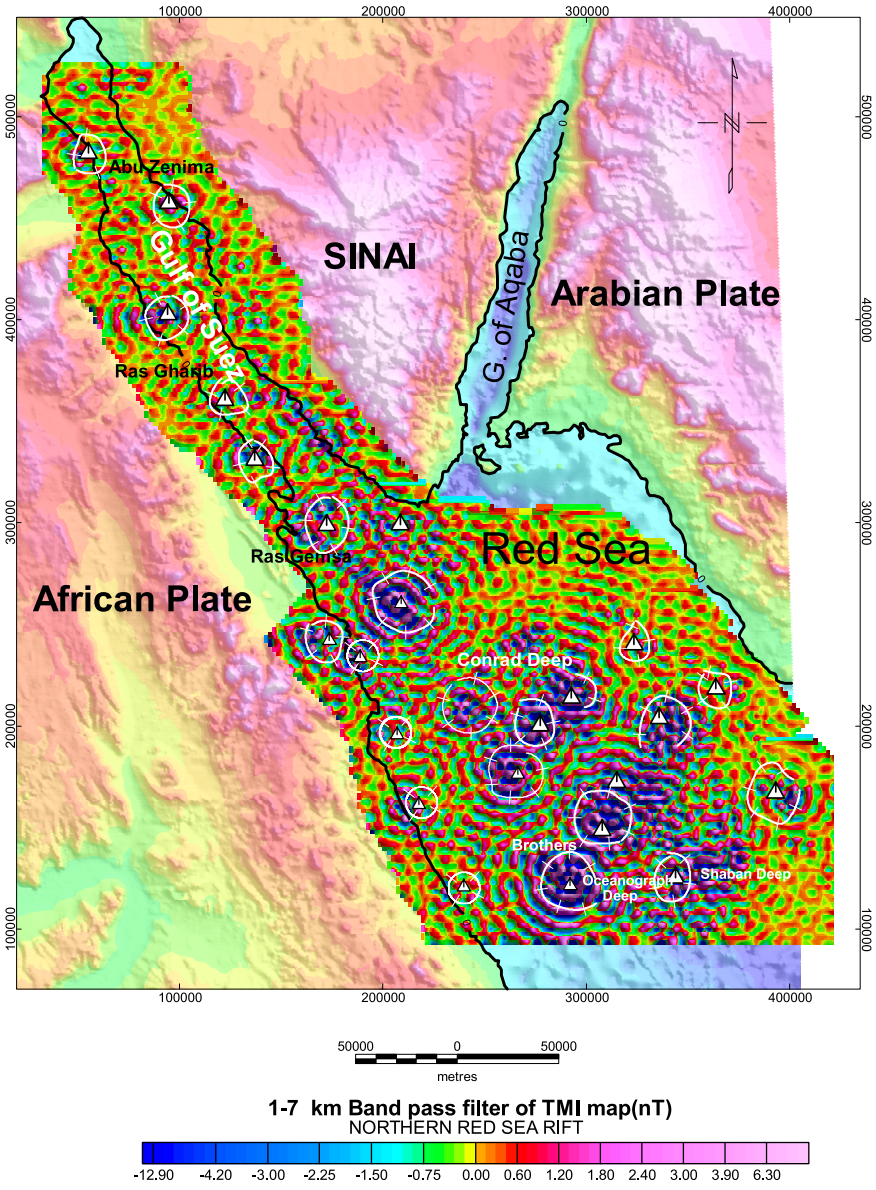

Fig. 9. 1–7 km band-pass filter of total magnetic intensity map overlain with interpreted intrusions. Both white triangles and circles mark location of volcanoes identified from filtered map.

mation of mid-oceanic ridges had not begun. In some places, an offset of the linear magnetic anomalies is evident (Fig. 10). These discontinuities or offsets are interpreted as marking the location of transform faults representing planes of differential horizontal extension across the sea floor spread. Five such faults are mapped (Figs. 10 and 11, faults from A to E marked by bold red lines). The northernmost transform is considered as the southern extension of the Dead Sea-Aqba transform. The azimuth of this transform fault is about 25°. The next three transform faults to the south show a more or less parallel trend to the northern transform, with azimuth ranging between 25 and 30. The azimuth of these transform faults agrees very well with the transform faults predicted with poles of rotation, as suggested by *Freund (1970)* and *Girdler and Darracott (1972)*. However, Red Sea axial segmentations are presented by yellow strip lines (in Fig. 11) and the circular anomalies which are signed by white triangles are interpreted as magmatic intrusions. In general, the Red Sea area is characterized by NW–SE trending faults, parallel to the Red Sea rift and NE–SW transform faults perpendicular to the Red Sea rift and in the direction of rifting. Moreover, the continental-oceanic crust boundary (Figs. 10 and 11) is also estimated using this study with their exact depth (4–5 km depth).

NE–SW Transform faults are marked by several interfering dipole anomalies, which represented intruded basaltic outcrops (volcanic bodies). The dipolar magnetic anomalies from these volcanoes merge together to form a NE–SW trending linear high-low pair (Fig. 11).

Generally, the seismicity map of Fig. 2 indicates a concentration of activity near latitudes, 27.6°, 26.5° and 26.0°N along the transform faults in the deep axial trough of the northern Red Sea.

Blank (1977) showed that the distribution of epicenters seems to be confined to narrow linear belts coinciding with the axial trough and north-east trending fracture zones. The estimated intruded bodies along transform fault "A and C" are accompanied with high seismic activity, while as, the intruded bodies along transform faults "B, D and E" are accompanied with low seismic activity. These results suggest that the tectonic activity of the Northern Red Sea is not controlled by simple stretching and symmetrical extension along a central axis. We can conclude that, the associations of basic intrusions with different activity along the transforms confirm the idea that the change in the motion of Arabia relative to Nubia (Africa), between

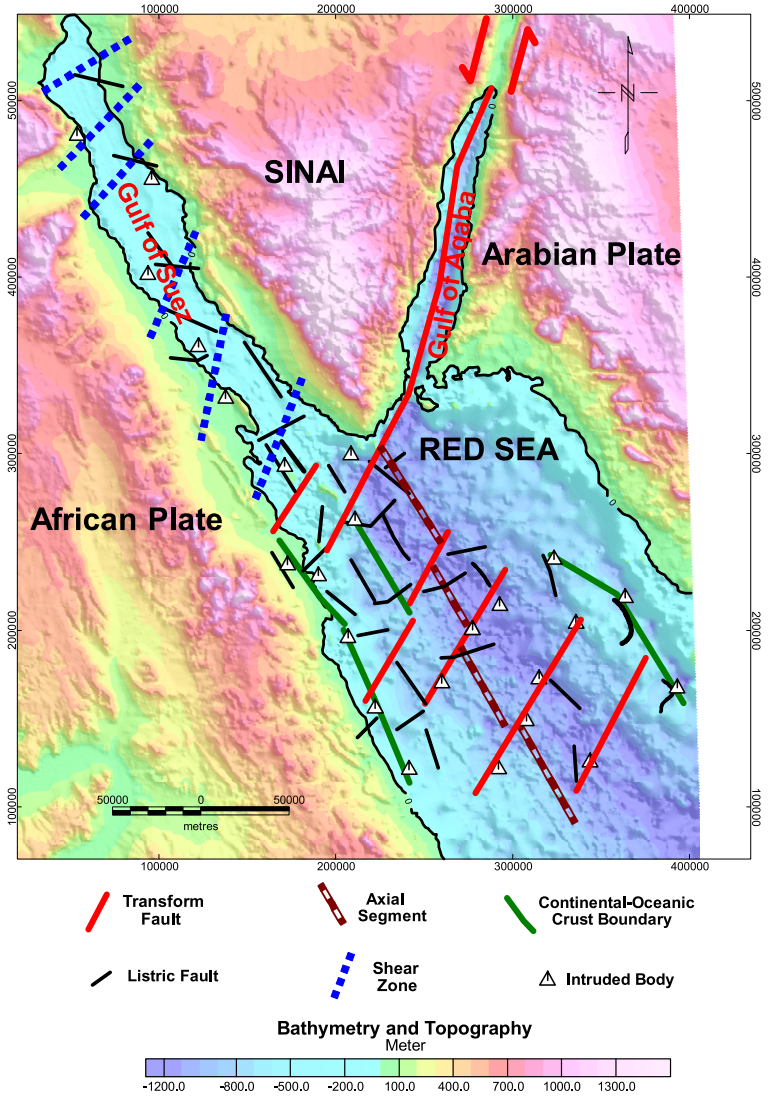

Fig. 10. Interpretation for northern Red Sea rift region derived from magnetic data analysis (from Euler Solutions resulting structural index contact model map (Fig. 6) with band pass filtered map (Fig. 9)). Six tectonic provinces were evaluated divided by six shear zones (dashed blue lines) passing the Suez rift. The map shows location of the transform faults resulting from our data analysis (NE red parallel heavy lines), as well as the location of the related volcanic intrusions (white triangles). Also the segmentation at the axial depression of Red Sea rift (brown strip lines), continental-oceanic crust boundary (heavy green lines) and listric normal faults (thin black lines) are identified.

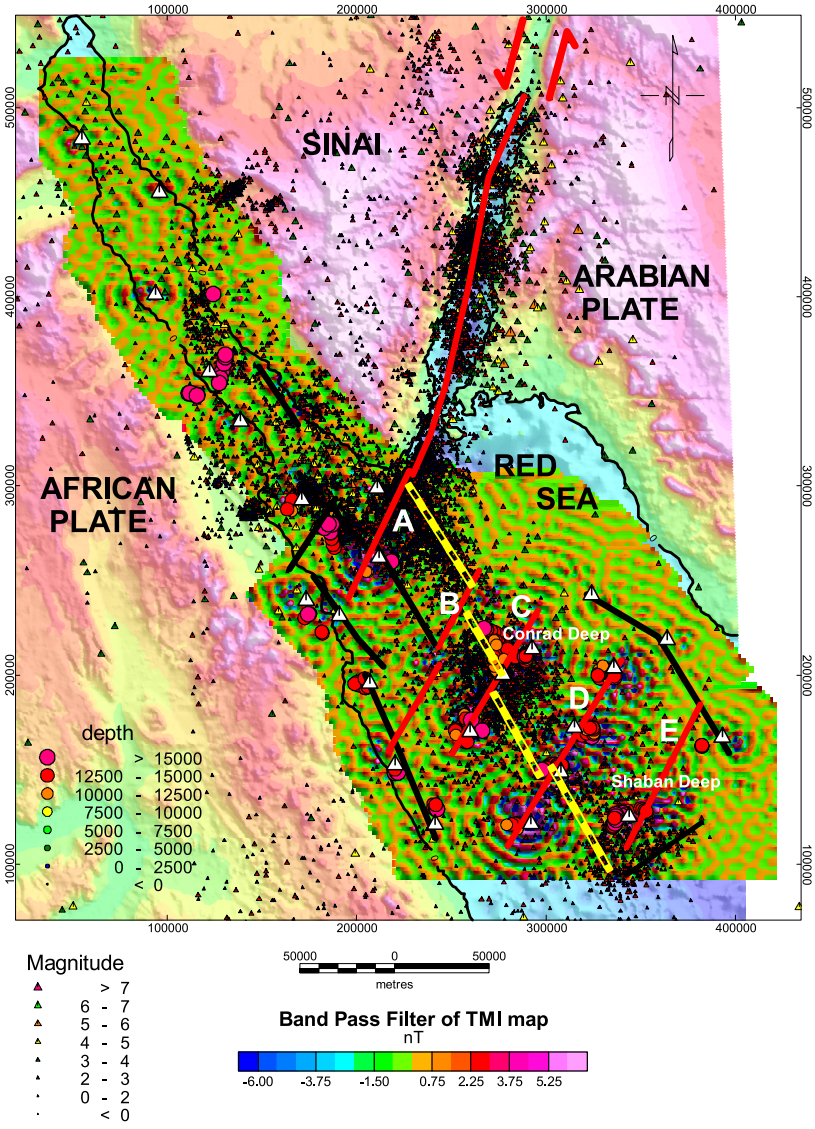

Fig. 11. Interpretation for northern Red Sea rift region from magnetic analysis (Euler Solutions resulting structural index of dipole model with band pass filter) and earthquake distributions with colored triangles. The map shows location of the Transform faults (A–E) (NE red parallel heavy lines) with their seismic activity, as well as the location of the related volcanic intrusions (white triangles). Also the segmentation at the axial depression of Red Sea rift (yellow strip lines) and continental-oceanic crust boundary (bold black lines) are identified.

the early and the recent spreading events.

5.1.3. Gravity source-contacts

The area under study is very large and in order to utilize the Euler solutions appropriately one needs to look at these solutions within small areas. The present study, however, does indicate that one could derive valuable information from Euler solutions. Euler 3D solutions of the gravity anomaly map over Red Sea rift region does not depict some of the important active sources brought out by the magnetic solutions (e.g. Volcanic intrusions and Transform faults) resulted from rifting.

However, the gravity Euler 3D solutions clearly bring out the contact between the sedimentary and the crystallines, listric faults throughout the border of Red Sea and the boundary thrust of the pull apart basins of Gulf of Aqaba. The Red Sea axial segmentations and boundary fault has its signature on the magnetic as well as Bouguer gravity solutions.

Interpretation of density source - contacts was also done using Euler solution of Bouguer data (Fig. 12). Good clustering of the solutions obtained shows dominant deep structural trends in NNW–SSE and NW–SE directions (orientation of the early Red Sea rift) which were affected by stretching and rifting processes. These trends can be traced across the Arabian Peninsula and gradually formed the proto-Red Sea trough *(Richter et al., 1991)*.

As the minor solutions are clustering in E–W (Ragabat El- Naam fault system) and N–S (East African rift System) directions. E–W trend acts as a front for the Syrian Arc structures at Sinai and Eastern Desert while as the N–S direction (East African rift System) was observed along the River Nile regions. Geologically, Sinai area is considered to be a major tectonic province controlled by trends of the Red Sea, Gulf of Suez and Gulf of Aqaba rifts *(Abu El Izz, 1971)*.

Ben-Avraham (1985) has recognized that the E–W shear zone (Ragabat El- Naam) acts as a front for the Syrian Arc structures.

Numerous bounding faults throughout the sedimentary section are shown in Fig. 13, due to block rotation associated with opening of the Red Sea and stretching and thinning of the continental crust, some of them were also expected in the Euler deconvolution Bouguer map (Fig. 11) along the Arabian and Egyptian Red Sea margins.

Euler solution maps (Figs. 6 and 12) agree well with the previous stud-

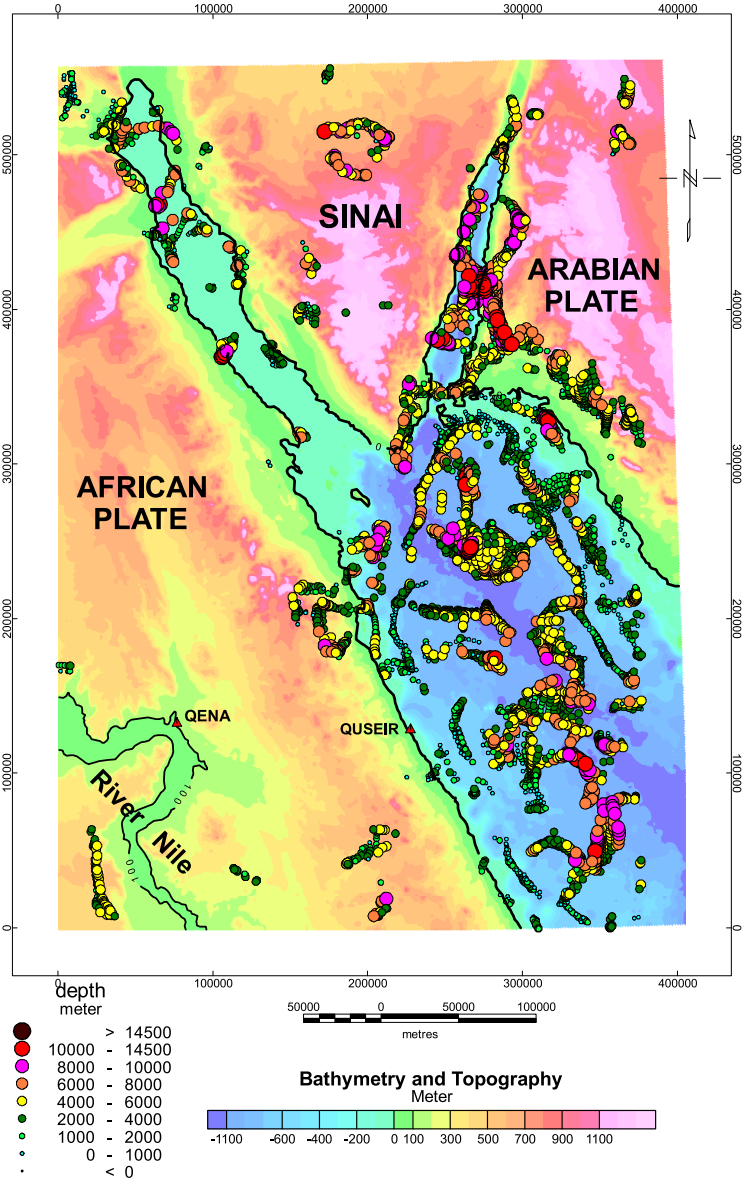

Fig. 12. Solutions of the 3D Euler method from the DED modification (Derivative Euler Deconvolution) for Bouguer data resulting structural index of contact model.

ies (e.g., *Bosworth et al., 1998; McClay and Khalil, 1998; Cochran, 2005*) which confirms attendance of alternative deep and shallow basement tectonic events (magnetic sources) trending NNW, NNE, N–S, and E–W. The combined effect of these tectonic events led to intense structuring and break-up into an enormous number of fault blocks composed of formation ranging in age from Precambrian to Eocene.

Deep sources (8–14 km depth) are systematically located on the seaward bathymetric deeps (series of deeps e.g. Conrad deep, Brothers and Shaban deep), and their origin may be sourced due to activity of Red Sea axial depression (Fig. 12).

Deep contact sources throughout the axial rift region are evident indicating the existence of highly magnetized sources. In particular, relationship of volcanoes to high seismic activity is well observed throughout the axial deeps (Figs. 6 and 12). The Euler source bodies of crustal contact (Fig. 12) reveal conspicuous tectonic feature located at northern part for Gulf of Aqaba defined pull-apart basins (the largest basin in the Gulf) between left-lateral strike slip faults of Dead Sea system. The depth investigation of these fault contacts (using 3D Euler deconvolution technique) is noticed to be changeable in their depths (ranged from 2.5 to more than 14 km depth). The basin appears to be divided into three separate units at depth *(Ben-Avraham, 1985)*. Also, the circle plot of the basement dykes and sills (Fig. 13) reveals a number of dykes and sills of shallower origin (5–10 km depth) occupying the located parallel and near to the coastal line of Red Sea followed by a small number of dykes of deeper origin locating on the central of Sinai, north most of Gulf of Suez, and on Gulf of Aqaba. Figure 14 is the interpretation map for northern Red Sea rift region resulted from Bouguer Euler solution with band bass filter techniques. The map shows location of the suggested continental-oceanic crust boundary (green heavy lines), as well as the location of the related fault blocks. PAB = Pull-Apart Basins of Gulf of Aqaba (blue lines, three basins were recognized: 1, 2 and 3).

Figure 15 is the resulted structural map for northern Red Sea rift region from all available geophysical data analyses in the present work (Bouguer and magnetic Euler solutions, band-pass filter of total magnetic intensity data and seismicity). The map shows location of all structures resulting from our data analysis (Figs. 6 to 14). Six tectonic provinces were evaluated divided by six shear zones (dashed blue lines) passing the Suez rift

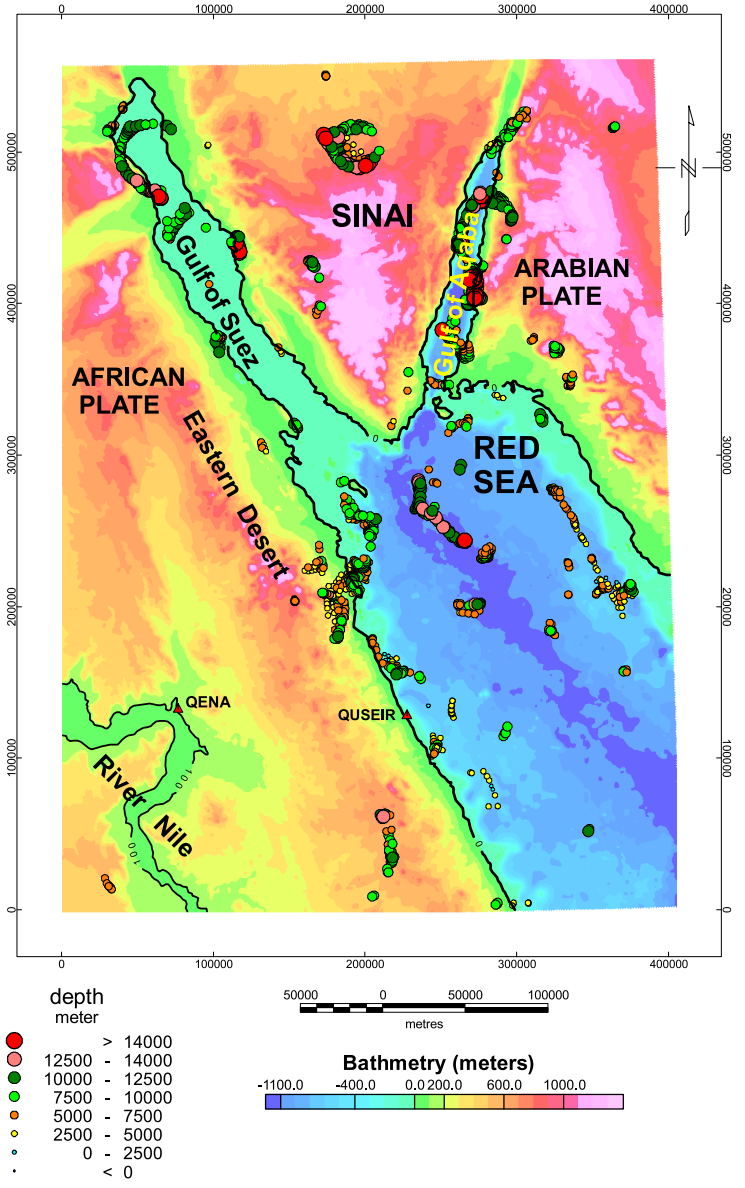

Fig. 13. Solutions of the 3D Euler method from the DED modification (Derivative Euler Deconvolution) for Bouguer data resulting structural index of sheets (dike and sills) model.

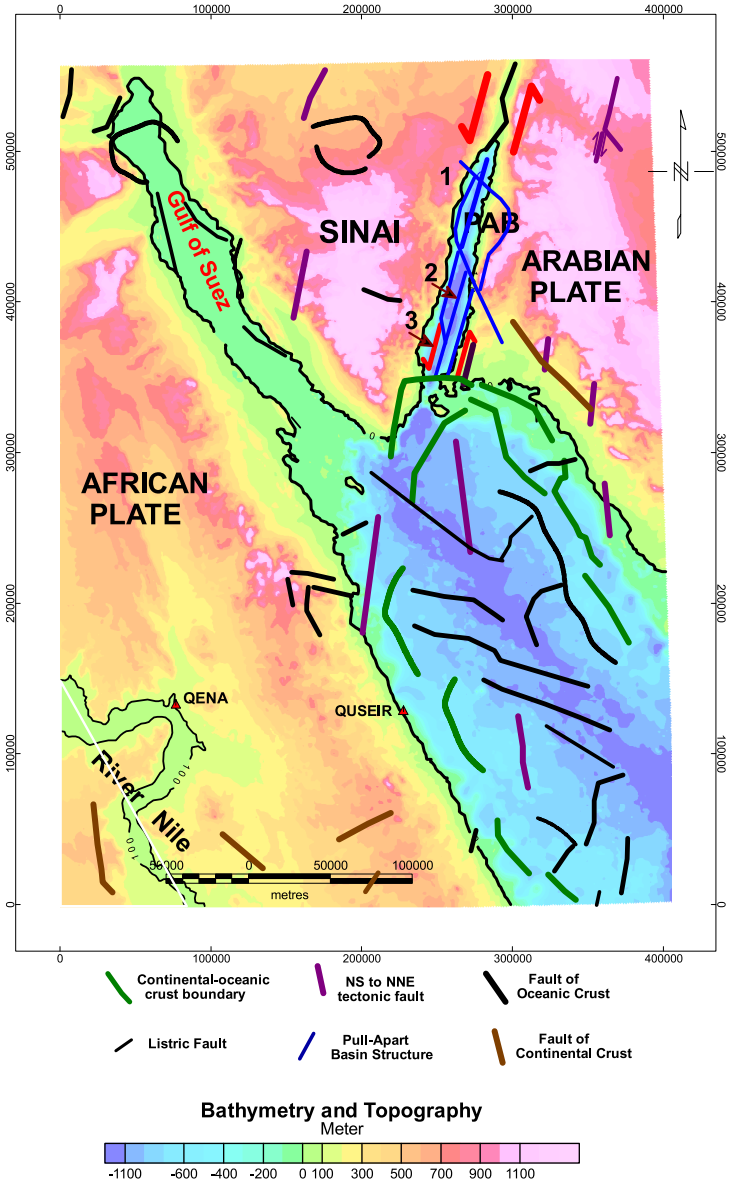

Fig. 14. Interpretation for northern Red Sea rift region from Bouguer Euler solution. The map shows location of the suggested continental-oceanic crust boundary (green heavy lines), as well as the location of the related fault blocks. PAB = Pull-Apart Basins of Gulf of Aqaba (blue lines, three basins were recognized (1, 2 and 3) from en echlon rhomb-shaped grabens produced by strike slip *(Ben-Avraham et al., 1979)*.

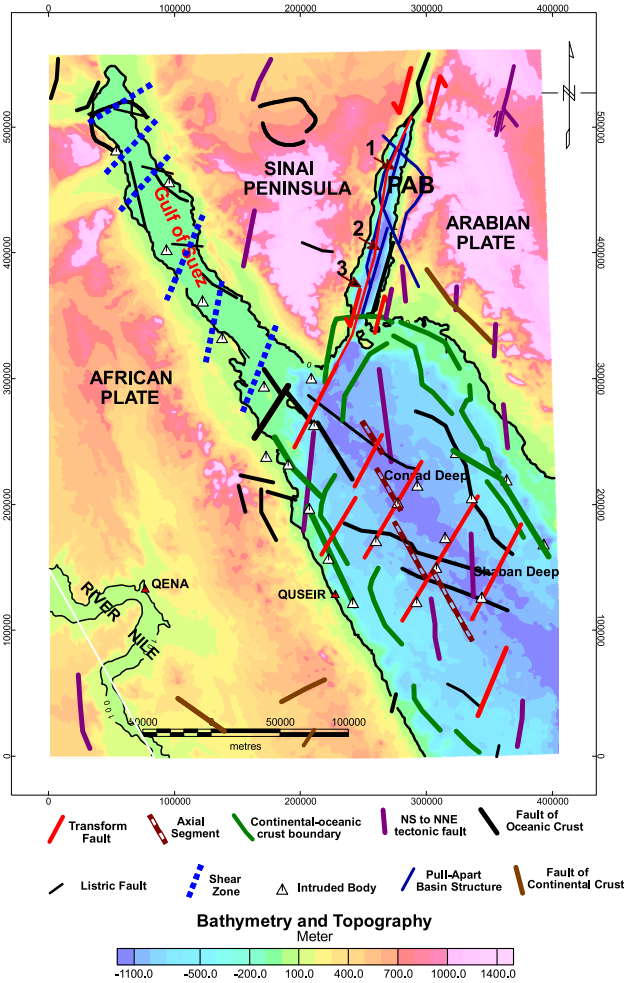

Fig. 15. Interpretation for northern Red Sea rift region from all available geophysical data analysis in the present work (Bouguer and magnetic Euler solution, band-pass filter of total magnetic intensity map and seismicity). The map shows location of all structures resulting from our data analysis (Figs. 6 to 14). Six tectonic provinces were evaluated divided by six shear zones (dashed blue lines) passing the Suez rift and many parallel transform faults (NE red parallel heavy lines), as well as the location of the related volcanic intrusions (white triangles). Also the segmentation at the axial depression of Red Sea rift (brown strip lines), continental-oceanic crust boundary (heavy green lines), listric normal faults (thin black lines) and faults of continental crust (brown lines) are identified. PAB = Pull-Apart Basins of Gulf of Aqaba (blue lines, three basins were recognized (1, 2 and 3) from en echlon rhomb-shaped grabens produced by strike slip *(Ben-Avraham et al., 1979)*.

and many parallel transform faults (NE red parallel heavy lines), as well as the location of the related volcanic intrusions (white triangles). Also the segmentation at the axial depression of Red Sea rift (brown strip lines), continental-oceanic crust boundary (heavy green lines), listric normal faults (thin black lines) and faults of continental crust (brown lines) are identified. PAB = Pull-Apart Basins of Gulf of Aqaba (blue lines, three basins were recognized (1, 2 and 3) from en echlon rhomb-shaped grabens produced by strike slip *(Ben-Avraham et al., 1979)*.

6. Discussion and conclusions

In this paper, we presented a case study of structural mapping using geophysical data of northern Red Sea, Egypt. The study provides information about buried subsurface structures with the help of the Euler method and bandpass filter maps.

Using filters in magnetic data enhances the data and helps defining features that were difficult to detect before filters.

Integrated interpretation of the geologic-geophysical, seismicity and topographic data reveals the elements of subsurface structure in the study area. Close correlation between the deep faults, seismicity and geomorphic expression at surface indicates their recent activity and control over sedimentation.

Several transform faults striking NE–SW (normal to the spreading axis of the northern Red Sea) were inferred from Euler deconvolution and bandpass of Total Magnetic intensity maps are marked by several interfering dipole anomalies. Results of the study were able to delineate circular magmatic bodies (volcanic extrusions) depicted from bandpass filter magnetic map (with average depth 10 to more than 18 km) scattered along specific tectonic features of the study area (their locations are well correlated with *Meneisy, 1990; Plaziat et al., 1998* and *Cochran, 2005*). These bodies are most probably representing intrusions associated with the Red Sea rift, indicating that their source is the heated anomalous upper mantle, which consequently confirms the idea that the asthenospheric upwelling might be responsible for the subsequent rifting of the Red Sea. Moreover, the study area is affected by sets of faults systems, which are mainly trending in the

NNW–SSE, NW–SE and NE–SW directions. As shown earlier, the constancy of the locations of the step faults and the dykes and sills indicates that the igneous activities generated are upwelled through the fissures and faults to form a number of dykes and sills dissecting most of Red Sea and Gulf of Suez regions.

The gravity, magnetic and heat flow are consistent with the interpretation that the extension and thinning which had been distributed across the rift becomes increasingly localized near the center of the now symmetric rift resulting in the formation of the axial depression.

As the extension and lithospheric thinning increased, the extension which had been accompanied by very small amounts of volcanism in the Gulf of Suez and marginal areas of the northern Red Sea begins to occur through intrusion of large igneous bodies.

These intrusions result in the formation of the northern Red Sea deeps which with further intrusion appears to serve as nucleation points for the seafloor spreading cells which grow and joint to form the mid-ocean ridge.

There is general agreement that the estimated intruded bodies are initiated from three different tectonic sources associated with the Red Sea rift. The results obtained using our data analysis confirm some of aspects (see *Coleman and McGuire, 1988*). Consequently, their locations within the northern Red Sea systematically occur at three distinct locations (tectonic features): a) there is a set of intruded bodies located on the edge of bathymetric terraces immediately adjacent to the continental-oceanic crust boundary of Red Sea rift and marginal area close to the Red Sea and Gulf of Suez rift. b) magmatic intrusions distributed across the rift and became focused to the area of the axial depression. c) Finally, some active intruded bodies are associated with the tectonic activity on most transform faults resulted from rifting of northern Red Sea. In addition, the alignment of the magmatic intrusions with the strike of the Gulf of Aqaba points to a weakness zone (faults) in the basement parallel to the Dead Sea Transform, the main tectonic structure in the Middle East, i.e., the magmatic activity was probably controlled by a fault structure in the basement that is parallel to the Dead Sea Transform. Distributions of seismic activity associated with some intruded bodies suggest that tectonic activity of the Northern Red Sea is not controlled by simple stretching and symmetrical extension along the axial trough.

Acknowledgments. We would like to express our gratitude to the General Petroleum Company, Cairo, for utilizing the Bouguer gravity data. Also, we would like to thank M. Hussein, Institute of Petroleum Research, for his encouragement and providing magnetic data. Roman Pašteka was supported by the Slovak Research and Development Agency under contract no. APVV-0194-10 and by Vega grant agency under projects no. 1/0095/12 and 2/0067/12. We thank anonymous reviewers for their thorough, critical and constructive comments that greatly contributed to improving this work.

References

Abu Al-Izz M. S., 1971: Land Forms of Egypt. The American University in Cairo press, Dar Al Maaref, Cairo, Egypt.

Abuzeid H. I., 1988: The youngest Precambrian volcanic succession of Wadi Hamrawein, Eastern desert, Egypt. PhD. Thesis., Earth Sc. And Res. Inst. South Carolina, Columbia, USA.

Badawy A., Mohamed A. M. S, Abu-Ali N., 2008: Seismological and GPS constraints on Sinai sub-plate motion along the Suez rift. Studia Geod. Geophys., **52**, 3, 397–412.

Baranov V., 1957: A new method for interpretation of aeromagnetic maps: Pseudo-gravimetric anomalies. Geophysics, **22**, 359–383.

Ben-Avraham Z., Almagar G., Garfunkel Z., 1979: Sediments and structure of the Gulf of Elat (Aqaba), northern Red Sea. Sediment. Geol., **23**, 239–267.

Ben-Avraham Z., 1985: Structural framework of the Gulf of Elat (Aqaba), Northern Red Sea. Geophysical Research, **90**, 703–726.

Ben-Menahem A., Nur A., Vered M., 1976: Tectonics, seismicity and structure of the Afro-Eurasian junction – the breaking of an incoherent plate. Phys. Earth Planet. Inter., **12**, 1–50.

Blank H. R., Jr., 1977: Aeromagnetic and geologic study of tertiary dikes and related structures on the Arabian margin of the Red Sea, in Red Sea research 1970-1975: Saudi Arabian Directorate General of Mineral Resources Bulletin, 22, G1–G18.

Bonatti E., Clocchiatti R., Colantoni P., Gelmini R., Marinelli G., Ottonello G., Santacroce R., Taviani M., Abdel-Meguid A. A., Assaf H. S., El Tahir M. A., 1983: Zabargad (St. John's) Island: An uplifted fragment of sub-Red Sea lithosphere. J. Geol. Soc. London, **140**, 4, 677–690.

Bosworth W., Taviani M., 1996: Late Quaternary reorientation of stress field and extension direction in the southern Gulf of Suez, Egypt: Evidence from uplifted coral terraces, mesoscopic fault arrays, and borehole breakouts. Tectonics, **15**, 791–802.

Bosworth W., Darwish M., Crevello P., Taviani M., Marshak S., 1996: Stratigraphic and structural evolution of Zabargad Island (Red Sea, Egypt) since the early Cretaceous. In: Proceedings of the Third International Conference on the Geology of the Arab World, edited by S. A. Youssef, Cairo Univ., 161–190.

Bosworth W., Strecker M., 1997: Stress field changes in the afro-arabian rift system during the Miocene to recent period. Tectonophysics, **278**, 47–62.

Bosworth W., Crevello P., Winn Jr., R. D., Steinmetz J., 1998: Structure, sedimentation, and basin dynamics during rifting of the Gulf of Suez and northwestern Red Sea. In: Purser B. H., Bosence D. W. J. (Eds.), Sedimentation and Tectonics of Rift Basins: Red Sea – Gulf of Aden. Chapman and Hall, London, 77–96.

Bosworth W., McClay K., 2001: Structural and stratigraphic evolution of the Gulf of Suez rift, Egypt: A synthesis. In: Ziegler P. A., Cavazza W., Robertson A. H. F., Crasquin-Soleau S., (Eds.), Peri-Tethys Memoir 6: Peri-Tethyan Rift/Wrench Basins and Passive Margins, Me'moires du Muse'um National d_Histoire Naturelle de Paris, **186**, 567–606.

Buck W. R., Martinez F., Steckler M. S., Cochran J. R., 1988: Thermal consequences of lithospheric extension: Pure and simple. Tectonics, **7**, 213–234.

Cochran J. R., 1983: A model for the development of the Red Sea. AAPG Bull., **67**, 41–69.

Cochran J. R., 2005: Northern Red Sea: Nucleation of an oceanic spreading center within a continental rift, G3 (Geochemistry, Geophysics, Geo-systems). An electronic Journal of the Earth Sciences, **6**, 3.

Cochran J. R., Martinez F., 1988: Evidence from the northern Red Sea on the transition from continental to oceanic rifting. Tectonophysics, **153**, 25–53.

Cochran J. R., Martinez F., Steckler M. S., Hobart M. A., 1986: Conrad deep: a new northern Red Sea deep. Origin and implications of continental rifting. Earth. Planet Sci. Lett., **78**, 18–32.

Coleman R. G., McGuire A. V., 1988: Magma systems related to the Red Sea opening. Tectonophysics, **150**, 1-2, 77–100.

Cooper G. R. J., Cowan D. R., 2006: Enhancing potential field data using filters based on the local phase. Computers and Geosciences, **32**, 1585–1591.

Daggett P., Morgan H., Boulos P., Hennin F. K., El-Sherif S. F., El-Sayed A. A., Basta N. Z., Melek Y. S., 1986: Seismicity and active tectonics of the Egyptian Red Sea margin and the northern Red Sea. Tectonophysics, **125**, 313–324.

Dmitriev V. I., Morozov V. A., Zhdanov M. S., Nikitin A. A., Brusnetzov N. P., Pavlov B. M., 1990: Numerical Mathematics and Techniques in Exploration Geophysics. Nedra, Moscow (in Russian).

El Shazly E. M., Saleeb Roufaiel G. S., Zaki N., 1974: Quaternary Basalt in Saint John's Island, Egypt. J. Geol., **18**, 2, 137–148.

El-Gezeery M. V., Marsouk I. M., 1974: Miocene rock stratigraphy of Egypt. Egypt. J. Geol., **18**, 1–59.

Fedi M., Florio G., 2001: Detection of potential fields source boundaries by enhanced horizontal derivative method. Geophysical Prospecting, **49**, 40–58. (doi:10.1046/j.1365-2478.2001.00235.x)

Fedi M., Florio G., 2002: Euler Deconvolution with no a priori definition of Structural Index. Geophysical Research Abstracts, **4**. European Geophys. Soc. 27th General Assembly, Nice, April, 21-26.

FitzGerald D., Reid A. B., McInerney P., 2004: New discrimination techniques for Euler deconvolution. Computers and Geosciences, **30**, 461–469.

Francheteau J., Lepichon X., 1972: A plate kinematic model of the Red Sea area. C.O.B., Brest, internal report.

Freund R., 1970: Plate tectonics of the Red Sea and Africa. Nature **228**, 453 p.

Girdler R. W., 1970: A review of the Red Sea heat flow. Philos. Trans. R. Soc. London, Ser. A, 267, 191–203.

Girdler R. W., Darracott B. W., 1972: African poles of rotation. Comments on Earth Sciences: Geophysics, **2**, 131–138.

Girdler R. W., Evans T. R., 1977: Red Sea heat flow. Geophys. J. the Roy. Astr. Soc., **51**, 245–251.

Guennoc P., Pautot G., Coutelle A., 1988: Surficial structures of the northern Red Sea axial valley from 23°N to 28°N: Time and space evolution of neo-oceanic structures. Tectonophysics, **153**, 1–23.

Guennoc P., Pautot G., Le Quentric M.-F., Coutelle A., 1990: Structure of an early oceanic rift in the northern Red Sea. Oceanol. Acta, **13**, 145–155.

Haenel R., 1972: Heat flow measurements in the Red Sea and the Gulf of Aden. Z. Geophys., **38**, 1035–1047.

Hartman R. R., Teskey D. J., Friedberg J., 1971: A system for rapid digital aeromagnetic interpretation. Geophysics, **36**, 891–918.

Hsu S., 2002: Imaging magnetic sources using Euler's equation. Geophysical Prospecting, **50**, 15–25.

Jackson J. A., White N. J., Garfunkel Z., Anderson H., 1988: Relations between normal-fault geometry, tilting and vertical motions in extensional terrains: an example from the southern Gulf of Suez. Journal of Structural Geology, **10**, 155–170.

Korrat I. M., Hussein H. M., Marzouk I., Ibrahim E. M., Abdel-Fattah R., Hurukawa N., 2006: Seismicity of the northernmost part of the Red Sea (1995-1999) Acta Geophysica, **54**, 1, 33–49, doi: 10.2478/s11600-006-0004-0.

Le Pichon X., Gaulier J. M., 1988: The rotation of Arabia and the Levant fault system. Tectonophysics, **153**, 271–294.

Martinez F., Cochran J. R., 1988: Structure and tectonics of the northern Red Sea: catching a continental margin between rifting and drifting. Tectonophysics, **150**, 1–32.

Martinez F., Cochran J. R., 1989: Geothermal measurements in the northern Red Sea: Implications for lithospheric thermal structure and mode of extension during continental rifting. J. Geophys. Res., **94**, 12,239–12,266.

McClay K., Khalil M. H., 1998: Extensional hard linkages, eastern Gulf of Suez, Egypt. Geology, **26**, 563–566.

McKenzie D. P., Davies D., Molnar P., 1970: Plate tectonics of the Red Sea and east Africa. Nature, **226**, 243–248.

Meneisy M. Y., 1990: Vulcanicity, in The Geology of Egypt, edited by R. Said, A. A. Balkema, Brookfield, Vt., 157–172.

Meshref W. M., 1990: Tectonic framework. In: Said, R. (Ed.), The Geology of Egypt, A. A. Balkema, Rotterdam, 113–155.

Mushayandebvu M. F., van Driel P., Reid A. B., Fairhead J. D., 2001: Magnetic source parameters of two-dimensional structures using extended Euler deconvolution. Geophysics, **66**, 814–823.

Mushayandebvu M. F., Lesur V., Reid A. B., Fairhead J. D., 2004: Grid Euler deconvolution with constraints for 2D structures. Geophysics, **69**, 489–496.

Nabighian M. N., 1972: The analytic signal of two-dimensional magnetic bodies with polygonal cross-section: Its properties and use for automated anomaly interpretation. Geophysics, **37**, 507–517.

Nabighian M. N., 1974: Additional comments on the analytic signal of two-dimensional magnetic bodies with polygonal cross-section. Geophysics, **39**, 85–92.

Nabighian M. N., 1984: Toward a three-dimensional automatic interpretation of potential field data via generalised Hilbert transforms: Fundamental relations. Geophysics, **49**, 780–786.

Nabighian M. N., Hansen R. O., 2001: Unification of Euler and Werner deconvolution in three dimensions via the generalized Hilbert transform. Geophysics, **66**, 1805–1810.

Naudy H., 1971: Automatic determination of depth on aeromagnetic profiles. Geophys., **36**, 717–722.

Nicolas A., Boudier F., Montigny R., 1987: Structure of Zabargad Island and early rifting of the Red Sea. J. Geophys. Res., **92**, 461–474.

Pašteka R., Richter F. P., Karcol R., Brazda K., Hajach M., 2009: Regularized derivatives of potential fields and their role in semi-automated interpretation methods. Geophysical Prospecting, **57**, 4, 507–516.

Pawlowski R. S., Hansen R. O., 1990: Gravity anomaly separation by Wiener Filtering. Geophysics, **55**, 539–548.

Piersanti A., Nostro C., Riguzzi F., 2001: Active displacement field in the Suez-Sinai area: the role of postseismic deformation. Earth and Planetary Science Letters, **193**, 13–23.

Plaziat J.-C., Baltzer F., Choukri A., Conchon O., Freylet P., Orszag-Sperber F., Raguideau A., Reyss J.-L., 1998: Quaternary marine and continental sedimentation in the northern Red Sea and Gulf of Suez (Egyptian coast): influences of rift tectonics, climatic changes and sea-level flucuations. In: Purser B. H., Bosemce D. W. J., eds., Sedimentation and Tectonics of Rift Basins: Red Sea – Gulf of Aden: Cambridge, Chapman and Hall, 537–573.

Reid A. B., Allsop J. M., Granser H., Millett A. J., Somerton I. W., 1990: Magnetic interpretation in three dimensions using Euler Deconvolution. Geophysics, **55**, 80–90.

Richter H., Makris J., Rim R., 1991: Geophysical observations offshore Saudi Arabia: seismic and magnetic measurements. Tectonophysics, **198**, 297–310.

Roest W. R., Verhoef J., Pilkington M., 1992: Magnetic interpretation using the 3D analytic signal. Geophysics, **57**, 116–12.

Said R., 1962: The Geology of Egypt. Elsevier Publ. Co, Amsterdam and New York.

Salamon A., Hofstetter A., Garfunkel Z., Ron H., 1996: Seismicity of the Eastern Mediterranean region: Perspective from the Sinai subplate. Tectonophysics, **263**, 293–305.

Saleh S., Jahr T., Jentzsch G., Saleh A., Abou Ashour N. M., 2006: Crustal evaluation of the northern Red Sea rift and Gulf of Suez, Egypt from geophysical data: 3-dimensional modelling. Journal of African Earth Sciences **45**, 257–278.

Salem A., Ravat D., 2003: A combined analytic signal and Euler method (AN-EUL) for the automatic interpretation of magnetic data. Geophysics, **68**, 1952–1961.

Salem A., Williams S., Fairhead J. D., Ravat D., Smith R., 2007: Tilt-depth method: A simple depth estimation method using firstorder magnetic derivatives. The Leading Edge, **26**, 1502–1505.

Shukri N. M., 1944: Geology of the Brothers Islets. Bull. Egypt. Fac. Sci., **75**, 175–196.

Stavrev P., 1997: Euler deconvolution using differential similarity transformations of gravity or magnetic anomalies. Geophysical Prospecting, **45**, 207–246.

Stavrev P., Reid A., 2007: Degrees of homogeneity of potential fields and structural indices of Euler deconvolution. Geophysics, **72**, L1–L12.

Steckler M. S., Berthelot F., Lyberis N., LePichon X., 1988: Subsidence in the Gulf of Suez: Implications for rifting and plate kinematics. Tectonophysics, **153**, 249–270.

Steckler M. S., Feinstein S., Kohn B. P., Lavier L. L., Eyal M., 1998: Pattern of mantle thin-ning from subsidence and heat flow measurements in the Gulf of Suez: Evidence for the rotation of Sinai and along-strike flow from the Red Sea. Tectonics, **17**, 903–920.

Taviani M., Bonatti E., Colantoni P., Rossi P., 1984: Tectonically uplifted crustal blocks in the northern Red Sea: Data from the Brothers islets. Mem. Soc. Geol. Ital., **27**, 47–50.

Tealeb A., Riad S., 1986: Regional tectonics of Sinai Peninsula interpreted from gravity and deep seismic data. In: Proceedings Fifth Annual Meeting of Egyptian Geophysical Society, Cairo, 18–49.

Thompson D. T., EULDEPTH 1982: A new technique for making computer assisted depth from magnetic data. Geophysics, **47**, 31–37.

Tikhonov A. N., Arsenin B. J., 1977: Solutions of Ill-posed Problems. John Wiley& Sons.

Werner S., 1953: Interpretation of magnetic anomalies of sheet-like bodies: Sveriges Geologiska Undersökning, Årsbok, **43**, 6.

Wijns C., Perez C., Kowalczyk P., 2005: Theta Map: Edge detection in magnetic data. Geophysics, **70**, L39–L43.